





Self-consistent description of high-spin states in doubly magic ^{208}Pb N. Lyutorovich ¹, V. Tselyaev ¹, J. Speth ², G. Martinez-Pinedo ^{3,4,5}, K. Langanke ^{3,4} and P.-G. Reinhard ⁶¹*St. Petersburg State University, St. Petersburg, 199034, Russia*²*Institut für Kernphysik, Forschungszentrum Jülich, D-52425 Jülich, Germany*³*GSI Helmholtzzentrum für Schwerionenforschung, Planckstraße 1, 64291 Darmstadt, Germany*⁴*Institut für Kernphysik (Theoriezentrum), Fachbereich Physik, Technische Universität Darmstadt, Schlossgartenstraße 2, 64298 Darmstadt, Germany*⁵*Helmholtz Forschungsakademie Hessen für FAIR, GSI Helmholtzzentrum für Schwerionenforschung, Planckstraße 1, 64291 Darmstadt, Germany*⁶*Institut für Theoretische Physik II, Universität Erlangen-Nürnberg, D-91058 Erlangen, Germany*

(Received 8 November 2021; accepted 14 January 2022; published 31 January 2022)

We analyze recent data on a long series of high-spin states in ^{208}Pb with a self-consistent phonon-coupling model for nuclear excitations based on the Skyrme functionals. The model is the renormalized time-blocking approximation which takes the coherent one-particle–one-hole states of the random-phase approximation (RPA) as starting point to develop more complex configurations beyond RPA. To the best of our knowledge, this is the first investigation of high spin states in ^{208}Pb using self-consistent nuclear models. The interesting point here is that complex configurations are compulsory to describe the upper end of the long spin series at all. The data thus provide an ideal testing ground for phonon-coupling models as they give direct access to complex configurations. We find that standard Skyrme functionals which perform well in ground state properties and giant resonance excitations deliver at once an agreeable description of these high spin states.

DOI: [10.1103/PhysRevC.105.014327](https://doi.org/10.1103/PhysRevC.105.014327)**I. INTRODUCTION**

High-spin states in nuclei show a rich variety of phenomena as, e.g., deformation alignment, back-bending, pairing breakdown, Coriolis antipairing, having thus attracted much attention in the past, for reviews see [1–3]. High-spin states in the doubly magic ^{208}Pb are special in that the large proton and neutron shell gaps inhibit deformation and pairing. A description in terms of an expansion into one-particle–one-hole (1p1h) states in a space including the complete neutron and proton shells $1\hbar\omega$ above and below the Fermi surface is limited approximately to angular momentum $I \leq 14$ because the angular momenta in these shells cannot supply more. The only way to couple to higher angular momenta are complex configurations. This renders high-spin states in ^{208}Pb to be a unique laboratory to study complex configurations without 1p1h background. The topic was taken up in a recent paper [4] which presents new experimental data up to spin $I = 30$ together with a theoretical analysis within large-scale shell model calculations which are particularly suited to deal with complex configurations. These shell model calculations consider one proton and one neutron shell below and another proton and neutron shell above the Fermi surface as valence space, tune the single-particle (s.p.) energies to the experimental spectra of the neighboring odd nuclei, and use a microscopic two-body interaction. It describes the experimental findings over the whole range of spins and it allows to get insight into the structure of the states: states up,

approximately, to $I = 13$ are described by 1p1h configurations while spins up to $I = 26$ are dominated by 2p2h configurations and higher by 3p3h configurations.

The aim of this paper is to see to what extent self-consistent models can describe the measured series of high-spin states in ^{208}Pb . Self-consistent mean-field models on the basis of effective energy-density functionals (EDF) manage to describe a wide range of nuclear-structure properties and excitations, for reviews see [5–7]. Excited states are usually described by the random-phase approximation (RPA) employing consistently the same EDF as was used to prepare the ground state. The RPA states are coherent superpositions of 1p1h configurations. One way to include more complex configurations is either to consider 2p2h configurations explicitly [8] or to use phonon coupling models where the 1p1h bases is coupled to nuclear “phonons” which are themselves the more collective from the RPA states [9–11]. One of the major successes is that phonon-coupling models provide a pertinent description of the spreading widths and consequently deliver realistic strength distributions for nuclear giant resonances, see, e.g., [12]. Still, the gross features of the resonances particularly their average position are determined by RPA in connection with proper choice of the EDF [13].

However, there are also states beyond reach of mere RPA. An example is the low-lying two-phonon states [14–17]. Studies of such states beyond RPA within a self-consistent description are so far scarce, although they provide an important further testing ground for nuclear EDFs. As argued above,

high-spin states in ^{208}Pb are another welcome test case where we need to look beyond RPA. We will do this using the recently developed renormalized time-blocking approximation (RenTBA) [18] which is a phonon-coupling model based on $1p1h \otimes$ phonon configurations where the phonons are self-consistently optimized (renormalized) within the RenTBA loop. RenTBA is a further developed version of the time-blocking approximation (TBA) [19,20] taking into account the single-particle continuum as described in Refs. [21–23]. The upper end of the spin series of [4], namely $I \geq 27$, goes even beyond the $1p1h \otimes$ phonon space. For these states we take into account $2p2h \otimes$ phonon configurations in an approximate RenTBA, denoted RenTBA₀.

II. THEORETICAL FRAMEWORK

The calculations were made first in RenTBA [18] where the coupling between two $1p1h \otimes$ phonon configurations was realized through the RPA propagator entering the Bethe-Salpeter equation for the response function taking into account the single-particle continuum (see [18,21–23]). RenTBA optimizes the phonons self-consistently within its own TBA scheme (not taking simply phonons from RPA calculations). This allows to achieve high quality with fewer basis phonon states which reduces computations expense and the danger of double counting.

For the high-spin states in ^{208}Pb with $13 \lesssim I < 27$, the $1p1h \otimes$ phonon configurations lie energetically in the nucleon continuum. Thus the coupling between them is mediated by the continuum part of the RPA response function, for details see Appendix 1. The continuum states couple only weakly to higher configurations. As a result, the uncoupled $1p1h \otimes$ phonon basis states are already a good approximation to the final result.

Thus we introduce an approximate RenTBA₀ where the coupling is neglected. This becomes particularly simple for the energies which then read

$$E_{phv} = \varepsilon_p - \varepsilon_h + \omega_v, \quad (1)$$

where the ε_a are the s.p. energies from the ground state EDF calculations and ω_v the eigenenergies of the RenTBA phonons (which can be determined independently from the high-spin states). The renormalization of the effective interaction is mediated here exclusively through the phonon energy ω_v .

We have calculated the energies of the ^{208}Pb states with $13 \leq I < 27$ both in the framework of the full-scale RenTBA (calculating the strength functions of electric and magnetic excitations) and in the RenTBA₀. The results of both the versions for the most of these states (excluding only mixed $1p1h + 1p1h \otimes$ phonon states: see the penultimate paragraph in Sec. III) have appeared surprisingly close. The energies obtained by the methods differ by about 0.01 MeV, which makes it possible to combine these methods for identification of the structure of states.

The RenTBA₀ then allows us to proceed to the upper end of the high-spin series with $I \geq 27$. This requires $2p2h \otimes$ phonon configuration which cannot be treated in RenTBA without substantial extension of the scheme. An obvious generalization of RenTBA₀ is to consider an uncoupled $2p2h \otimes$

phonon whose energy is then simply

$$E_{pp'hh'v} = \varepsilon_p + \varepsilon_{p'} - \varepsilon_h - \varepsilon_{h'} + \omega_v. \quad (2)$$

As RenTBA₀ worked so well for $I < 27$, we expect reliable predictions also for the higher spins. Thus we show in the following results for RenTBA up to $I = 26$ and for RenTBA₀ for larger I .

The technical details of the calculations were as follows. Wave functions and fields were represented on a spherical grid in coordinate space. The s.p. basis was discretized by imposing a box boundary condition with a box radius equal to 18 fm. To check that the results do not depend on the box size, some calculations were also performed with the box radius = 27 fm. The particle's energies ε_p were limited by the maximum value $\varepsilon_p^{\text{max}} = 100$ MeV. The details of solving the nonlinear RenTBA equations are described in Ref. [24]. To find the energies of the states, the strength functions $S(E)$ were calculated with very small smearing parameters ($\Delta = 1$ keV, some times 0.1 keV or even less) and the energies were read off from the maxima in the $S(E)$.

The calculations employed Skyrme EDF with three parameter sets. The set SV-bas is chosen because it provides a good description of properties of many nuclei (see [25]). The choice of the spin-spin part of the EDF leaves several options open [26]. But spin-spin interactions may be important for the excitations with unnatural parity which we also consider here. We choose the most extensive option to include all spin terms and fix them by the assumption as if the EDF is derived from the expectation value of the same zero-range momentum-dependent two-body Skyrme force as the SV-bas [26], thus without any new parameters. This straightforward extension, although successful for describing odd nuclei [26], is found to be somewhat insufficient for low lying magnetic modes, a problem which was solved by slightly modifying spin terms and spin-orbit force of the EDF [24,27]. We consider here two of these modified functionals used in our calculations, namely SV-bas_{-0.44} and SKXm_{-0.49}. The first is a variant of SV-bas from [25] and the second of SKXm from [28]. The modification was designed to describe the nuclear ground-state properties with approximately the same accuracy as the original SKXm and SV-bas and to reproduce at the same time the basic experimental characteristics of the $M1$ excitations in ^{208}Pb within the RenTBA. We have yet to see how the performance of unnatural parity states with higher spin comes out.

III. RESULTS AND DISCUSSION

The results for the ^{208}Pb high-spin states are presented in Figs. 1 and 2, where I and π denote spin and parity of a state, E are experimental and theoretical energies (in MeV). The experimental values were taken from [4,29] and the shell model values from [4]. In some cases the spin and parity assignments of levels do not coincide between Refs. [4] and [29], namely the 7.974, 8.027, and 9.061 MeV levels. In these cases, we preferred the identification [4], since it is the later one. Our calculations confirm the correctness of this choice. The RenTBA energies calculated using the SV-bas, SV-bas_{-0.44}, and SKXm_{-0.49} parameter sets are shown in

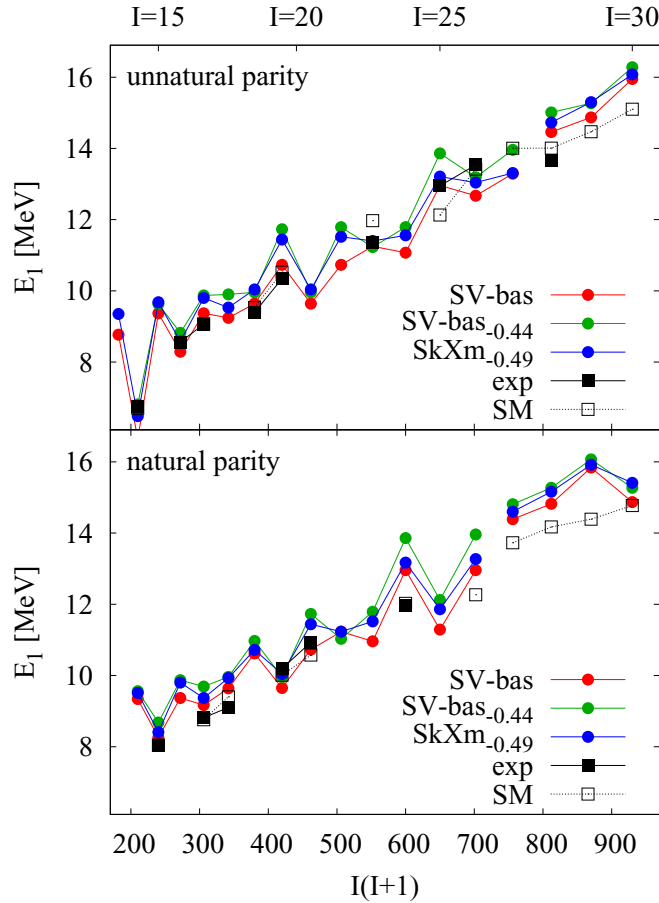


FIG. 1. Energies E_1 of ^{208}Pb yrast states plotted versus $I(I+1)$ for the spins $13 \leq I \leq 30$ computed with RenTBA for three different Skyrme parametrizations as indicated and compared with available experimental data as well as with shell model calculations (indicated by “SM”) [4]. The lower panel shows results for natural parity states and the upper panel for unnatural parity states. On the lower panel, the lines are interrupted between $I = 26$ and $I = 27$ to indicate that the high I states have a different structure ($2p2h \otimes \text{phonon}$). On the upper panel, the change appears between $I = 27$ and $I = 28$.

the figures by red, green, and blue dots connected by lines of the same colors. The experimental energies are shown in filled black squares and the shell model results in open black squares. The experimental data are surprisingly well described by all mean-field based models. In particular, the trend with spin I is well reproduced. One can see, however, that within the three mean-field parametrizations the SV-bas has a slight preference in spite of the fact that the SV-bas_{0.44} and SKXm_{0.49} produce the improved spin residual interaction. The reason is that the low-lying 1^+ phonons and the respective $1p1h$ energies in the ^{208}Pb which were used in the fit of the parameters of the SV-bas_{0.44} and SKXm_{0.49} sets do not enter the configurations relevant for the high-spin states, see Appendix 2. The shell model (open black squares) performs usually a bit better than SV-bas. But there are also cases where SV-bas wins. Taken over all, both models are competitive.

Finally, we remark that the general trend looks very much like a rotational band, though the experimental trend in de-

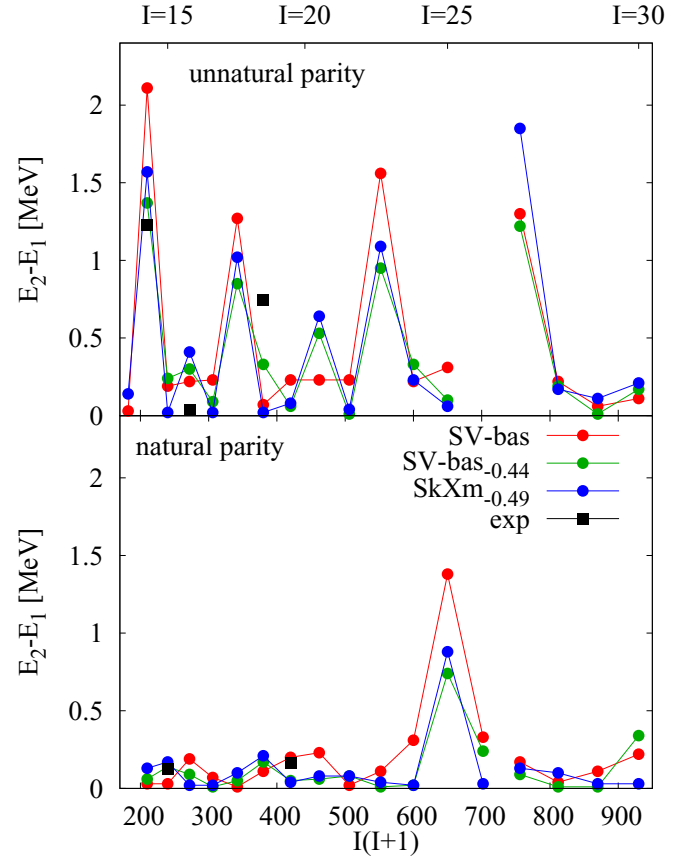


FIG. 2. As in Fig. 1, but for the energy difference $E_2 - E_1$ for the first two excited states in each angular momentum I channel.

tail does not always follow exactly a straight line (E is approximately constant in the ranges $I = 17-18$ and $26-28$). Nevertheless, taken over all, both experimental and theoretical trends are similar to a rotational band. However, this band does not rely on a collective rotation in the sense of cranking [30]. This is hindered by the spherical shape and the large shell gap of ^{208}Pb . It is not excluded to find a representation in terms of a rotating exotic deformation coupled to $1p1h$ states as was proposed, e.g., in [31] for the high-spin states in the 6 MeV region. Our analysis of the microscopic structure shows that the high-spin states are of predominantly s.p. structure, composed from combinations of s.p. states and phonons with high spin. The rotational trend stems from a change in the angular momentum of one single nucleon at a time where the rotational part of the s.p. kinetic energy gives a large contribution to the s.p. energy, for quantitative details see Appendix 2. In practice, our calculations show that the 13_1^- and 14_1^- states have still mixed $1p1h + 1p1h \otimes \text{phonon}$ structure while the states with spins $13 \leq I \leq 26$ (including 13_2^- and 14_2^- but except 26_2^-) are predominantly $1p1h \otimes \text{phonon}$ configurations and the even larger I need $2p2h \otimes \text{phonon}$ configurations. The 26_2^- state is at the transition point. The energy of its $1p1h \otimes \text{phonon}$ configuration is 15.16 MeV which is higher than the 13.51 MeV of the $2p2h \otimes \text{phonon}$ state (values for SV-bas). The latter is then the relevant configuration.

The data in [4] allow also to deduce a few values for the second excited state. Drawing them together with the RenTBA results looks very much like Fig. 1 for the first excited state, a near linear trend with $I(I+1)$ and acceptable agreement with theory. We do not show that here to avoid doubling. Rather we take an amplifying glass and look in Fig. 2 at the energy difference between second and first excited states. All three Skyrme parametrizations yield the same trend, however with occasional visible quantitative differences. The few experimental data basically agree with the theoretical values, except for $I=18$. Unfortunately the data are still too sparse to be conclusive.

IV. CONCLUSIONS

In this paper, the energies of the high-spin yrast and near-yrast states in ^{208}Pb have been calculated within a fully self-consistent approach beyond RPA taking into account 1p1h and 1p1h \otimes phonon configurations. The approach is based on the Skyrme energy-density functional (EDF) and on the recently developed renormalized version of the time-blocking approximation (RenTBA) [18]. The results are compared to the recent experimental data and shell model results [4]. The main conclusions of our calculations are as follows:

- (1) The self-consistent approach based on the Skyrme EDF and the RenTBA gives reasonable agreement with the experimental energies of the high-spin yrast states in ^{208}Pb without refitting the parameters of the Skyrme EDF previously determined from the large-scale calculations of many nuclear properties.
- (2) The yrast states with the total angular momenta $15 \leq I \leq 26$ in ^{208}Pb can be interpreted with high accuracy as the pure 1p1h \otimes phonon configurations in our model, those with even higher spins as 2p2h \otimes phonon configurations which allows here to use the approximate treatment by RenTBA₀.
- (3) The energies of the phonons used in these 1p1h \otimes phonon configurations should be determined in the framework of the full-scale RenTBA that implies the solution of the system of nonlinear equations of this model.

ACKNOWLEDGMENTS

This work was supported by the Russian Foundation for Basic Research, Project No. 21-52-12035, and the Deutsche Forschungsgemeinschaft, Contract No. RE 322/15-1. This research was carried out using computational resources provided by the Computer Center of St. Petersburg State University.

APPENDIX: DETAILS ON THE HIGH-SPIN STATES

1. High spins and 1p1h or RPA states

All excited states in ^{208}Pb with spins $I \geq 15$ lie above the neutron and proton separation energies which are, e.g., $S_n = 7.58$ and $S_p = 7.94$ MeV for the SV-bas. Therefore, discrete RPA (DRPA) becomes inappropriate because the artificial

TABLE I. DRPA results for the energies (in MeV) of the high-spin yrast states of ^{208}Pb in comparison with the experimental data [4]. Here, r_b denotes the box radius (in fm) used in the DRPA calculations.

	Exp.	DRPA	
		$r_b = 18$	$r_b = 27$
$E(15_1^-)$	8.027	21.5	14.7
$E(17_1^+)$	9.061	23.6	15.6
$E(20_1^-)$	10.342	30.7	18.7
$E(20_1^+)$	10.196	33.3	19.9

quantization of continuum states by DRPA falsifies energies and strengths.

One signature of that is a strong dependence of these states on box size as illustrated in Table I for two values of the box radius r_b . The continuum RPA (CRPA) correctly takes into account the single-particle continuum for every I^π . However, the CRPA strength functions for the high-spin electric or magnetic excitations in ^{208}Pb have one dominant and very broad peak whose centroid is in the region above 20 MeV with a width of 15–25 MeV depending on the excitation. These centroid energies stay way above the experimental energies of the high-spin yrast states in ^{208}Pb that shows that mere RPA is unable to describe these data.

The continuum structure of 1p1h (or RPA) states has consequences for their coupling to 1p1h \otimes phonon states and for the coupling between the 1p1h \otimes phonon states. The 1p1h \otimes phonon configurations considered in our study and the matrix elements of the interaction between them and the 1p1h configurations are formed predominantly by the discrete and quasidiscrete s.p. states which are orthogonal or approximately orthogonal to the continuum states. For this reason the couplings mentioned above are weak. Nonetheless, the couplings between the 1p1h and 1p1h \otimes phonon states is necessary to provide the latter with some direct multipole strength. The resulting multipole strength function has very narrow peaks with the small integral strength in the vicinity of the energies of 1p1h \otimes phonon states and must be calculated there with high energy resolution.

2. Structure of phonons and complex states

Table II indicates the structure of the phonons in percentage 1p1h components whereby only sufficiently large components are shown. With few exceptions, states with high spins come close to pure 1p1h states while low-spin states are typically a superposition of many different 1p1h components. The latter can be called collective phonons while the high-spin states are noncollective phonons.

Table III shows the energies and structures of the high-spin excitations at the level of 2p2h, 1p1h \otimes phonon, and two-phonon states calculated with SKXm_{-0.49}. That makes it obvious that the states with very high spin are composed from s.p. states with high spin via phonons with high spins. It becomes also apparent that the states acquire increasingly

TABLE II. Composition of phonons up the highest spin which can be represented by mere RPA states. Only 1p1h components with sufficiently large contributions are given.

3_1^-	$= \nu 2g_{9/2} 3p_{3/2}^{-1} 22\% + \pi 1h_{9/2} 2d_{3/2}^{-1} 20\% + \dots$
4_1^+	$= \nu 2g_{9/2} 1i_{13/2}^{-1} 55\% + \pi 1h_{9/2} 1h_{11/2}^{-1} 14\%$
5_1^-	$= \nu 2g_{9/2} 3p_{1/2}^{-1} 81\%$
6_1^-	$= \nu 2g_{9/2} 3p_{3/2}^{-1} 80\% + \nu 2g_{9/2} 2f_{5/2}^{-1} 20\%$
6_1^+	$= \pi 1i_{13/2} 3s_{1/2}^{-1} 42\% + \nu 2g_{9/2} 1i_{13/2}^{-1} 25\%$
7_1^-	$= \nu 2g_{9/2} 2f_{5/2}^{-1} 98\%$
8_1^-	$= \nu 1i_{11/2} 2f_{5/2}^{-1} 99\%$
8_1^+	$= \nu 2g_{9/2} 1i_{13/2}^{-1} 83\%$
10_1^-	$= \pi 1i_{13/2} 1h_{11/2}^{-1} 54\% + \nu 1j_{15/2} 1i_{13/2}^{-1} 45\%$
10_1^+	$= \nu 2g_{9/2} 1i_{13/2}^{-1} 98\%$
11_1^+	$= \nu 2g_{9/2} 1i_{13/2}^{-1} 100\%$
12_1^-	$= \nu 1j_{15/2} 1i_{13/2}^{-1} 62\% + \pi 1i_{13/2} 1h_{11/2}^{-1} 38\%$
12_1^+	$= \nu 1i_{11/2} 1i_{13/2}^{-1} 100\%$
13_1^-	$= \nu 1j_{15/2} 1i_{13/2}^{-1} 100\%$
13_1^+	$= \nu 1j_{15/2} 1h_{11/2}^{-1} 88\%$
14_1^-	$= \nu 1j_{15/2} 1i_{13/2}^{-1} 100\%$

simple structures, the more so as the strength of the residual interaction decreases with increasing spin.

Table III also elucidates the generally rotational trend $E_I \propto I(I+1)$. The trend is the same for all levels of approach such that we can learn about the underlying structure already from the simple Np/Nh configurations. The trend is driven by a change in the angular momentum of one nucleon after the other. The spins of the high-spin yrast states are composed of single-particle states having large angular momentum. The rotational part of a s.p. kinetic energy gives a large contribution to the s.p. energy. Thus a change in the angular momentum of one nucleon produces a significant change in the excitation energy. This rotation is not collective but is a single-particle rotation. At first glance, it resembles the rotational alignment known from rotating deformed nuclei. However, the situation is different. Rotational alignment dissolves gradually the collective cranking rotations which then are replaced by a sequence of single-particle contributions. The doubly magic ^{208}Pb has a large spectral gap which inhibits cranking from the onset. The generation of rotational spectra by single-particle structures starts right away without a phase of collective rotations coming before.

 TABLE III. Energies and structures of 2p2h, 1p1h \otimes phonon, and two-phonon energies for high spins calculated with SKXm $_{-0.49}$. The energies were calculated for the renormalized phonons.

I_n^π	Exp.	2p2h		1p1h \otimes phonon		phonon \otimes phonon	
		E	Configuration	E	Configuration	E	Configuration
15_1^-	8.027	9.10	$\nu 2g_{9/2} 1i_{13/2}^{-1} \otimes \nu 2g_{9/2} 3p_{1/2}^{-1}$	8.41	$\nu 2g_{9/2} 3p_{1/2}^{-1} \otimes 10_1^+$	7.89	$10_1^+ \otimes 5_1^-$
15_1^+	^a	10.56	$\nu 1i_{11/2} 2f_{5/2}^{-1} \otimes \nu 2g_{9/2} 2f_{5/2}^{-1}$	9.68	$\nu 2g_{9/2} 1i_{13/2}^{-1} \otimes 4_1^+$	8.83	$12_1^- \otimes 3_1^-$
16_1^-	8.562 ^b	9.10	$\nu 2g_{9/2} 1i_{13/2}^{-1} \otimes \nu 2g_{9/2} 3p_{1/2}^{-1}$	8.58	$\nu 2g_{9/2} 3p_{1/2}^{-1} \otimes 11_1^+$	8.06	$11_1^+ \otimes 5_1^-$
16_1^+		10.70	$\nu 2g_{9/2} 1i_{13/2}^{-1} \otimes \pi 1i_{13/2} 3s_{1/2}^{-1}$	9.80	$\nu 1j_{15/2} 1i_{13/2}^{-1} \otimes 3_1^-$	8.87	$13_1^- \otimes 3_1^-$
17_1^-	8.8128	9.92	$\nu 2g_{9/2} 1i_{13/2}^{-1} \otimes \nu 2g_{9/2} 3p_{3/2}^{-1}$	9.36	$\nu 2g_{9/2} 2f_{5/2}^{-1} \otimes 10_1^+$	8.92	$11_1^+ \otimes 6_1^-$
17_1^+	9.061 ^a	11.67	$\nu 1j_{15/2} 1i_{13/2}^{-1} \otimes \nu 2g_{9/2} 3p_{3/2}^{-1}$	9.80	$\nu 1j_{15/2} 1i_{13/2}^{-1} \otimes 3_1^-$	9.17	$14_1^- \otimes 3_1^-$
18_1^-		10.06	$\nu 2g_{9/2} 1i_{13/2}^{-1} \otimes \nu 2g_{9/2} 2f_{5/2}^{-1}$	9.54	$\nu 2g_{9/2} 2f_{5/2}^{-1} \otimes 11_1^+$	9.22	$11_1^+ \otimes 7_1^-$
18_1^+	9.1030	10.70	$\nu 2g_{9/2} 1i_{13/2}^{-1} \otimes \pi 1i_{13/2} 3s_{1/2}^{-1}$	9.92	$\nu 2g_{9/2} 3p_{1/2}^{-1} \otimes 13_1^-$	9.35	$10_1^+ \otimes 8_1^+$
19_1^-	9.394	11.24	$\nu 1i_{11/2} 1i_{13/2}^{-1} \otimes \nu 2g_{9/2} 2f_{5/2}^{-1}$	10.71	$\nu 1i_{11/2} 2f_{5/2}^{-1} \otimes 11_1^+$	10.30	$11_1^+ \otimes 8_1^-$
19_1^+	9.394	10.73	$\nu 2g_{9/2} 1i_{13/2}^{-1} \otimes \nu 2g_{9/2} 1i_{13/2}^{-1}$	10.04	$\nu 2g_{9/2} 1i_{13/2}^{-1} \otimes 8_1^+$	9.35	$10_1^+ \otimes 10_1^+$
20_1^-	10.3419	12.39	$\pi 1i_{13/2} 1h_{11/2}^{-1} \otimes \nu 2g_{9/2} 1i_{13/2}^{-1}$	11.44	$\nu 2g_{9/2} 1i_{13/2}^{-1} \otimes 10_1^-$	10.75	$10_1^- \otimes 10_1^+$
20_1^+	10.1959	10.73	$\nu 2g_{9/2} 1i_{13/2}^{-1} \otimes \nu 2g_{9/2} 1i_{13/2}^{-1}$	10.04	$\nu 2g_{9/2} 1i_{13/2}^{-1} \otimes 10_1^+$	9.35	$10_1^+ \otimes 10_1^+$
21_1^-	10.9343	12.39	$\pi 1i_{13/2} 1h_{11/2}^{-1} \otimes \nu 2g_{9/2} 1i_{13/2}^{-1}$	11.44	$\nu 2g_{9/2} 1i_{13/2}^{-1} \otimes 10_1^-$	10.83	$12_1^- \otimes 10_1^+$
21_1^+		10.73	$\nu 2g_{9/2} 1i_{13/2}^{-1} \otimes \nu 2g_{9/2} 1i_{13/2}^{-1}$	10.04	$\nu 2g_{9/2} 1i_{13/2}^{-1} \otimes 10_1^+$	9.52	$11_1^+ \otimes 10_1^+$
22_1^-		12.39	$\nu 2g_{9/2} 1i_{13/2}^{-1} \otimes \pi 1i_{13/2} 1h_{11/2}^{-1}$	11.52	$\nu 2g_{9/2} 1i_{13/2}^{-1} \otimes 12_1^-$	10.83	$12_1^- \otimes 10_1^+$
22_1^+		11.91	$\nu 1i_{11/2} 1i_{13/2}^{-1} \otimes \nu 2g_{9/2} 1i_{13/2}^{-1}$	11.22	$\nu 1i_{11/2} 1i_{13/2}^{-1} \otimes 10_1^+$	10.78	$11_2^+ \otimes 11_1^+$
23_1^-		12.39	$\pi 1i_{13/2} 1h_{11/2}^{-1} \otimes \nu 2g_{9/2} 1i_{13/2}^{-1}$	11.52	$\nu 2g_{9/2} 1i_{13/2}^{-1} \otimes 12_1^-$	10.87	$13_1^- \otimes 10_1^+$
23_1^+	11.3609	11.92	$\nu 2g_{9/2} 1i_{13/2}^{-1} \otimes \nu 1i_{11/2} 1i_{13/2}^{-1}$	11.40	$\nu 1i_{11/2} 1i_{13/2}^{-1} \otimes 11_1^+$	11.27	$11_1^+ \otimes 12_1^+$
24_1^-		12.48	$\nu 2g_{9/2} 1i_{13/2}^{-1} \otimes \nu 1j_{15/2} 1i_{13/2}^{-1}$	11.56	$\nu 2g_{9/2} 1i_{13/2}^{-1} \otimes 13_1^-$	11.04	$11_1^+ \otimes 13_1^-$
24_1^+	11.9582	14.14	$\nu 1j_{15/2} 1i_{13/2}^{-1} \otimes \pi 1i_{13/2} 1h_{11/2}^{-1}$	13.17	$\pi 1i_{13/2} 1h_{11/2}^{-1} \otimes 12_1^-$	12.30	$12_1^- \otimes 12_1^-$
25_1^-		12.48	$\nu 1j_{15/2} 1i_{13/2}^{-1} \otimes \nu 2g_{9/2} 1i_{13/2}^{-1}$	11.86	$\nu 2g_{9/2} 1i_{13/2}^{-1} \otimes 14_1^-$	11.34	$14_1^- \otimes 11_1^+$
25_1^+	12.9493	14.14	$\pi 1i_{13/2} 1h_{11/2}^{-1} \otimes \nu 1j_{15/2} 1i_{13/2}^{-1}$	13.21	$\pi 1i_{13/2} 1h_{11/2}^{-1} \otimes 13_1^-$	12.34	$12_1^- \otimes 13_1^-$
26_1^-	13.5360	13.67	$\nu 1j_{15/2} 1i_{13/2}^{-1} \otimes \nu 1i_{11/2} 1i_{13/2}^{-1}$	13.04	$\nu 1i_{11/2} 1i_{13/2}^{-1} \otimes 14_1^-$	12.92	$14_1^- \otimes 12_1^+$
26_1^+		14.13	$\nu 1j_{15/2} 1i_{13/2}^{-1} \otimes \pi 1i_{13/2} 1h_{11/2}^{-1}$	13.27	$\nu 1j_{15/2} 1i_{13/2}^{-1} \otimes 12_1^-$	12.38	$13_1^- \otimes 13_1^-$
27_1^+		14.23	$\nu 1j_{15/2} 1i_{13/2}^{-1} \otimes \nu 1j_{15/2} 1i_{13/2}^{-1}$	13.31	$\nu 1j_{15/2} 1i_{13/2}^{-1} \otimes 13_1^-$	12.68	$14_1^- \otimes 13_1^-$

^aThe spin-parity assignment to the level 9.061 is (17^+) in the NDS [29] and 17^+ in Ref. [4] but 15^+ in Ref. [31].

^bThe level 8.562 is taken from Ref. [29].

- [1] M. J. A. de Voigt, J. Dudek, and Z. Szymański, *Rev. Mod. Phys.* **55**, 949 (1983).
- [2] J. X. Saladin, R. A. Sorensen, and C. M. Vincent, *High Spin Physics and Gamma-Soft Nuclei* (World Scientific, Singapore, 1991).
- [3] D. Ward and P. Fallon, in *Advances in Nuclear Physics*, edited by J. W. Negele and E. W. Vogt (Springer, Boston, 2001), pp. 167–291.
- [4] R. Broda, R. V. F. Janssens, L. W. Iskra, J. Wrzesinski, B. Fornal, M. P. Carpenter, C. J. Chiara, N. Cieplicka-Oryńczak, C. R. Hoffman, F. G. Kondev, W. Królas, T. Lauritsen, Z. Podolyak, D. Seweryniak, C. M. Shand, B. Szpak, W. B. Walters, S. Zhu, and B. A. Brown, *Phys. Rev. C* **95**, 064308 (2017).
- [5] M. Bender, P.-H. Heenen, and P.-G. Reinhard, *Rev. Mod. Phys.* **75**, 121 (2003).
- [6] D. Vretenar, A. V. Afanasjev, G. Lalazissis, and P. Ring, *Phys. Rep.* **409**, 101 (2005).
- [7] J. Erler, P. Klüpfel, and P. G. Reinhard, *J. Phys. G: Nucl. Part. Phys.* **38**, 033101 (2011).
- [8] S. Drożdż, S. Nishizaki, J. Speth, and J. Wambach, *Phys. Rep.* **197**, 1 (1990).
- [9] V. G. Soloviev, *Theory of Atomic Nuclei: Quasiparticles and Phonons* (Institute of Physics, Bristol and Philadelphia, 1992).
- [10] G. Colò and P. F. Bortignon, *Nucl. Phys. A* **687**, 282 (2001).
- [11] S. Kamenetzkiy, J. Speth, and G. Terentyev, *Phys. Rep.* **393**, 1 (2004).
- [12] N. Lyutorovich, V. I. Tselyaev, J. Speth, S. Krewald, F. Grümmer, and P. G. Reinhard, *Phys. Rev. Lett.* **109**, 092502 (2012).
- [13] P. Klüpfel, P. G. Reinhard, T. J. Bürvenich, and J. A. Maruhn, *Phys. Rev. C* **79**, 034310 (2009).
- [14] C. A. Bertulani and V. Y. Ponomarev, *Phys. Rep.* **321**, 139 (1999).
- [15] B. A. Brown, *Phys. Rev. Lett.* **85**, 5300 (2000).
- [16] E. Litvinova, P. Ring, and V. Tselyaev, *Phys. Rev. Lett.* **105**, 022502 (2010).
- [17] E. Litvinova, P. Ring, and V. Tselyaev, *Phys. Rev. C* **88**, 044320 (2013).
- [18] V. Tselyaev, N. Lyutorovich, J. Speth, and P.-G. Reinhard, *Phys. Rev. C* **97**, 044308 (2018).
- [19] V. I. Tselyaev, *Sov. J. Nucl. Phys.* **50**, 780 (1989).
- [20] V. I. Tselyaev, *Phys. Rev. C* **75**, 024306 (2007).
- [21] N. Lyutorovich, V. Tselyaev, J. Speth, S. Krewald, F. Grümmer, and P.-G. Reinhard, *Phys. Lett. B* **749**, 292 (2015).
- [22] N. Lyutorovich, V. Tselyaev, J. Speth, S. Krewald, and P.-G. Reinhard, *Phys. At. Nucl.* **79**, 868 (2016).
- [23] V. Tselyaev, N. Lyutorovich, J. Speth, S. Krewald, and P.-G. Reinhard, *Phys. Rev. C* **94**, 034306 (2016).
- [24] V. Tselyaev, N. Lyutorovich, J. Speth, and P.-G. Reinhard, *Phys. Rev. C* **102**, 064319 (2020).
- [25] P. Klüpfel, J. Erler, P.-G. Reinhard, and J. A. Maruhn, *Eur. Phys. J. A* **37**, 343 (2008).
- [26] K. J. Pototzky, J. Erler, P.-G. Reinhard, and V. O. Nesterenko, *Eur. Phys. J. A* **46**, 299 (2010).
- [27] V. Tselyaev, N. Lyutorovich, J. Speth, P.-G. Reinhard, and D. Smirnov, *Phys. Rev. C* **99**, 064329 (2019).
- [28] B. A. Brown, *Phys. Rev. C* **58**, 220 (1998).
- [29] M. Martin, *Nucl. Data Sheets* **108**, 1583 (2007).
- [30] P. Ring and P. Schuck, *The Nuclear Many-Body Problem* (Springer-Verlag, New York/Heidelberg/Berlin, 1980).
- [31] A. Heusler, *J. Phys.: Conf. Ser.* **1643**, 012137 (2020).